Journal of
Materials Chemistry C

PAPER

View Article Online
View Journal | View Issue

Cite this: *J. Mater. Chem. C*, 2019, 7, 2240

Published on 21 January 2019. Downloaded on 2/12/2026 3:28:52 PM.

Two spirobifluorene-based fluorescent probes with aggregation-induced emission properties: synthesis and application in the detection of Zn^{2+} and cell imaging†

Jianyong Wan,‡ Wu Zhang,‡ Hongda Guo, JingJing Liang, Danyu Huang and Haibo Xiao *

Received 3rd November 2018,
Accepted 18th January 2019

DOI: 10.1039/c8tc05526b

rsc.li/materials-c

In this work, two spirobifluorene-based probes, namely **SPF-1** and **SPF-2**, were designed and synthesized. They exhibited high selectivity and sensitivity toward Zn^{2+} with enhanced emissions, which could be attributed to the formation of an L–Zn complex. The detection limit of **SPF-2** is 63 nM for Zn^{2+} and this is significantly lower than most previous reports. **SPF-1** was successfully used for intracellular Zn^{2+} imaging. In addition, **SPF-2** possesses two-photon absorption properties and has been applied in two-photon fluorescence cell imaging. This study is the first time that a spirobifluorene-based probe with aggregation-induced emission enhancement (AIEE) properties has been reported. We hope that this molecular design triggers further interest in using spiro-configured compounds in AIEE-based bioprobes for further applications.

1. Introduction

Zinc(II) is the second most abundant transition metal ion in the human body and actively involved in diverse biological processes.[1,2] It constructs the catalytic active center of more than 300 enzymes as a cofactor, regulates protein and gene expression, and participates in neural signal transmission.[3] Disorders in zinc ion metabolism are associated with various diseases such as Alzheimer's, Parkinson's disease, cerebral ischemia, Menkes and familial amyotropic lateral sclerosis.[4,5] Therefore, it is crucial to develop fluorescent probes to detect the concentration of Zn^{2+}.[6]

Tang *et al.* reported aggregation-induced emission (AIE) or the aggregation-induced emission enhancement (AIEE) phenomenon in 2001.[7] AIEE fluorogens usually have rotor structures, and are weakly-emissive or non-emissive in solution, but exhibit very strong emission upon the formation of aggregates.[8] In the past few years, various AIEE-based chemosensors and biosensors have attracted significant attention owing to their potential use in real-world applications.[9] Up until now, a series of one- and two-photon absorption (TPA) fluorescent probes have been designed and synthesized, which possess excellent AIEE properties.[10–16]

Spirobifluorene appears to be a good fluorophore core for fluorescent probes owing to its inherent rigid structure that efficiently suppresses excimer formation, which is frequently encountered in the solid state or in concentrated solutions. A successful example of a spirobifluorene-based fluorescent probe was reported by K.-T. Wong *et al.* in 2011, for the specific detection of NO.[17] We have reported the design and synthesis of two-photon fluorescent probes based on the spirobifluorene motif for the first time.[18–20] These spirobifluorene-based fluorescence probes have high extinction coefficients and photoluminescence (PL) quantum yields. However, no spirobifluorene-based probe with AIEE properties has been reported previously.

Herein, we report two fluorescent probes based on the spirobifluorene motif (Scheme 1) for the detection of Zn^{2+} by

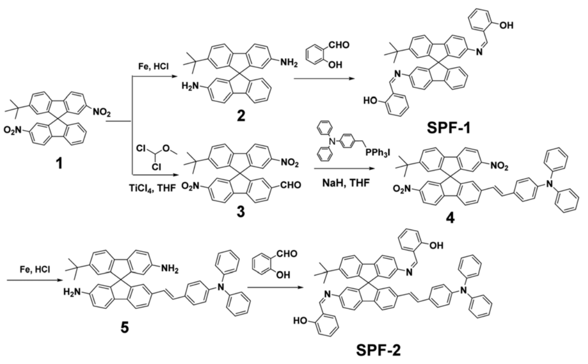

Scheme 1 The synthetic routes to **SPF-1** and **SPF-2**.

Department of Chemistry, Shanghai Normal University, Shanghai 200234, P. R. China. E-mail: xiaohb@shnu.edu.cn

† Electronic supplementary information (ESI) available. See DOI: 10.1039/c8tc05526b

‡ These authors made equal contributions to this work.

This journal is © The Royal Society of Chemistry 2019

Published on 21 January 2019. Downloaded on 2/12/2026 3:28:52 PM.

taking advantage of the AIEE feature. In addition, the applications in intracellular Zn^{2+} imaging and two-photon fluorescence cell imaging were investigated.

2. Experimental

2.1 Materials

The synthetic routes to **SPF-1** and **SPF-2** are shown in Scheme 1. Synthetic intermediates **1** and **2** were prepared according to our previously reported methods.[21] All chemicals were of analytical grade and were used as received.

2.2 Measurements

The melting points of the compounds were determined using WRX-4 microscope melting point apparatus. All nuclear magnetic resonance (NMR) spectra were obtained on a Bruker DRX 400 MHz spectrometer. Elemental analyses were performed using Atlantic Microlab. UV-Vis absorption spectra were determined using a Perkin Elmer Lambda 35 spectrophotometer. Fluorescence spectra were recorded on a Perkin Elmer LS55 instrument.

The TPA cross-section of **SPF-2** was measured at 800 nm using the open-aperture *Z*-scan technique using a high-power femtosecond laser (PHAROS High-Power Femtosecond Lasers sp). The pulse duration was about 190 fs (estimated as the full width half maximum (FWHM) of a Gaussian temporal profile). The light beam used was Top-hat and the focal length (f) was 250 mm. The TPA cross-section (σ) value can be calculated by using the equation: $\sigma = h\nu\beta N_0$, in which $N_0 = N_AC$ is the number density of the centers (N_A is the Avogadro constant, C represents the solute molar concentration), and β is the TPA coefficient.[22]

2.3 Living cell cultures and imaging

A549 cells were incubated in DMEM medium with 10% fetal bovine serum at 37 °C under a 5% CO_2 atmosphere. One day before the fluorescence imaging, the A549 cells were passaged and plated in 30 mm glass culture dishes. During the logarithmic growth phase, they were cultured to 50–70% culture fit in the presence of complete medium (2 mL). Afterwards, the cells on glass slides were washed with DMEM and fed with culture medium (contain 1% DMSO) containing the probe (50 μM) for 30 min at 37 °C under a 5% CO_2 atmosphere. Subsequently, A549 cells were washed with PBS solution three times. One of the groups cells stained with **SPF-1** was treated with 100 μM Zn^{2+} for another 30 min and washed three times with PBS solution.

Two-photon fluorescence cell images were taken on an Ultimal IV confocal microscope equipped with a femtosecond Ti:sapphire laser.

2.4 Preparation of the compounds

Synthesis of 2,2′-((1*Z*,1′*Z*)-((2′-(*tert*-butyl)-9,9′-spirobi[fluorene]-2,7′-diyl)bis(azanylylidene))bis(methanylylidene))diphenol (SPF-1). To a 50 mL flask, 0.402 g (1 mmol) **2**, 10 mL absolute ethyl alcohol, 5 mL ethyl acetate, and 0.22 mL (2.1 mmol) 2-hydroxybenzaldehyde were added. The mixture was stirred at room temperature for 1 h. The resulting precipitate was filtered and washed with cold ethanol and finally dried under vacuum. Yield 0.51 g (83.6%). MP: 243–245 °C. ^{1}H NMR (400 MHz, $CDCl_3$) 13.21 (s, 2H), 7.94 (d, J = 8.1 Hz, 1H), 7.89 (t, J = 8.1 Hz, 2H), 7.82 (d, J = 8.1 Hz, 1H), 7.50 (dd, J = 8.1, 1.7 Hz, 1H), 7.44 (t, J = 7.8 Hz, 1H), 7.39 (dd, J = 8.1, 1.8 Hz, 1H), 7.32 (q, J = 7.3, 5.6 Hz, 5H), 7.17 (t, J = 7.8 Hz, 1H), 6.97 (dd, J = 8.0, 2.5 Hz, 2H), 6.88 (td, J = 7.4, 2.7 Hz, 2H), 6.81 (d, J = 7.8 Hz, 2H), 6.81 (d, J = 7.8 Hz, 2H), 6.74 (s, 1H), 6.66 (s, 1H), 1.21 (s, 9H). ^{13}C NMR (101 MHz, $CDCl_3$) δ 161.77, 161.62, 161.17, 151.79, 150.43, 150.40, 149.13, 148.54, 148.02, 147.65, 141.09, 140.81, 140.76, 138.67, 133.03, 132.97, 132.21, 132.16, 128.09, 128.03, 125.51, 124.25, 121.95, 121.82, 120.91, 120.87, 120.61, 120.15, 119.64, 119.20, 118.99, 118.96, 117.21, 116.49, 116.32, 77.07, 76.76, 66.15, 35.01, 31.47. Elemental analysis (%) calcd for $C_{43}H_{34}N_2O_2$: C 84.56, H 5.61, N 4.59, O 5.24. Found: C 84.81, H 5.62, N 4.57.

Synthesis of 2′-(*tert*-butyl)-7,7′-dinitro-9,9′-spirobi[fluorene]-2-carbaldehyde (3). To a 250 mL flask, 3.2 g (6.96 mmol) compound **1** and 30 mL anhydrous dichloromethane were added under a nitrogen atmosphere. After the mixture was stirred at 0 °C for 10 min, a 30 mL CH_2Cl_2 solution of $TiCl_4$ (16 mL) and 20 mL CH_2Cl_2 solution of dichloro(methoxy)methane (4 mL, 4.2 mmol) were added dropwise over 30 min, respectively. The reaction mixture was continually stirred at room temperature for 24 h. Then, the mixture was poured into iced water and extracted using CH_2Cl_2 (20 mL × 3). The combined organic solution was washed with 50 mL saturated sodium bicarbonate solution and 50 mL water, respectively. The organic solvent was removed using a rotary evaporator. The residue was purified by column chromatography on silica (petroleum ether/ethyl acetate, 5 : 1, v/v) to give a yellow solid (1.56 g). Yield: 46.0%. MP: 175–178 °C. ^{1}H NMR (400 MHz, $CDCl_3$, δ): 9.91 (s, 1H), 8.40 (dd, J = 8.4, 2.0 Hz, 1H), 8.34 (dd, J = 8.4, 2.0 Hz, 1H), 8.14 (dd, J = 15.0, 8.2 Hz, 2H), 8.04 (dd, J = 8.0, 1.1 Hz, 1H), 7.98 (d, J = 8.5 Hz, 1H), 7.92 (d, J = 8.2 Hz, 1H), 7.59 (m, J = 9.0, 8.2 Hz, 2H), 7.47 (d, J = 2.0 Hz, 1H), 7.31 (s, 1H), 6.73 (s, 1H), 1.18 (s, 9H).

Synthesis of (*E*)-4-(2-(2′-(*tert*-butyl)-2,7′-dinitro-9,9′-spirobi-[fluoren]-7-yl)vinyl)-*N*,*N*-diphenylaniline (4). To a 50 mL flask, 0.123 g (0.25 mmol) **3**, 0.324 g (0.5 mmol) 4-((iodotriphenylphosphoranyl)methyl)-*N*,*N*-diphenylaniline, 0.03 g (0.75 mmol) NaH and 5 mL dried THF were added under a nitrogen atmosphere. Then, the mixture was stirred at 0 °C for 24 h. The solvent was evaporated, and the residue was subjected to column chromatography on silica gel eluting with petroleum ether and ethyl acetate (4 : 1, V/V) to give 98 mg of a red solid (yield 54%). MP: 155–158 °C. ^{1}H NMR (400 MHz, $CDCl_3$) δ 8.36 (ddd, J = 7.9, 5.6, 2.1 Hz, 2H), 8.03–7.92 (m, 4H), 7.65 (dd, J = 8.1, 1.5 Hz, 1H), 7.60 (dd, J = 8.2, 1.7 Hz, 1H), 7.56 (d, J = 2.0 Hz, 2H), 7.30 (d, J = 3.3 Hz, 1H), 7.27 (s, 2H), 7.25 (s, 1H), 7.13–6.97 (m, 10H), 6.95 (s, 1H), 6.90–6.79 (m, 3H), 1.22 (s, 9H).

Synthesis of (*E*)-7-(*tert*-butyl)-7′-(4-(diphenylamino)styryl)-9,9′-spirobi[fluorene]-2,2′-diamine (5). To a mixture of 0.366 g **4** (0.5 mmol) and 0.558 g iron powder (1 mmol) in 25 mL ethanol, 2 mL of concentrated hydrochloric acid was added dropwise over 30 min under a nitrogen atmosphere. After refluxing for 3 h,

Published on 21 January 2019. Downloaded on 2/12/2026 3:28:52 PM.

the solution was neutralized dropwise with NH_4OH solution, and the resulting precipitate was filtered off with suction. The solvent was evaporated, and the residue was purified by column chromatography (petroleum ether/ethyl acetate, 10 : 7, v/v) to afford 0.252 g of a yellow solid **5** (75%). MP: 181–183 °C. ^1H NMR (400 MHz, DMSO-*d*) 7.68 (d, *J* = 7.9 Hz, 1H), 7.63 (d, *J* = 8.0 Hz, 1H), 7.60–7.49 (m, 3H), 7.40 (d, *J* = 8.4 Hz, 2H), 7.40 (d, *J* = 8.4 Hz, 2H), 7.35–7.23 (m, 6H), 7.06–6.95 (m, 8H), 7.06–6.95 (m, 8H), 6.93 (s, 1H), 6.85 (d, *J* = 8.5 Hz, 2H), 6.69 (s, 1H), 6.57–6.51 (m, 3H), 5.85 (dd, *J* = 6.3, 2.0 Hz, 2H), 5.14 (d, *J* = 35.9 Hz, 4H), 1.10 (s, 9H).

Synthesis of 2,2′-((1*Z*,1′*Z*)-((2-(*tert*-butyl)-2′-((*E*)-4-(diphenylamino)styryl)-9,9′-spirobi[fluorene]-7,7′-diyl)bis(azanylylidene))-bis(methanylylidene))diphenol (SPF-2). To a 50 mL flask, 0.134 g (0.2 mmol) **5**, 15 mL absolute ethyl alcohol, 5 mL ethyl acetate, and 43.8 μL (0.42 mmol) 2-hydroxybenzaldehyde were added. The mixture was refluxed at 85 °C. The reaction progress was monitored on TLC. When the reaction was over (about 1 hour), the solvent was evaporated. A yellow solid was precipitated, which was filtered and washed with cold ethanol and finally dried under vacuum. Yield 0.138 g (79%). MP: 173–175 °C. ^1H NMR (400 MHz, $CDCl_3$) δ 13.2 (s, 2H), 8.52 (d, *J* = 5.9 Hz, 2H), 7.91 (dd, *J* = 8.1, 3.1 Hz, 2H), 7.86 (t, *J* = 8.0 Hz, 2H), 7.58 (dd, *J* = 8.1, 1.6 Hz, 1H), 7.52 (dd, *J* = 8.1, 1.8 Hz, 1H), 7.41–7.29 (m, 7H), 7.26–7.22 (m, 4H), 7.12–7.06 (m, 4H), 7.06–6.94 (m, 7H), 6.94–6.82 (m, 6H), 6.71 (dd, *J* = 7.3, 1.9 Hz, 2H), 1.22 (s, 9H). ^{13}C NMR (101 MHz, $CDCl_3$) δ 161.70, 161.63, 161.14, 151.87, 150.72, 150.44, 149.65, 148.54, 147.89, 147.75, 147.51, 147.34, 140.71, 140.56, 140.34, 138.69, 137.76, 133.02, 132.97, 132.18, 131.31, 129.28, 128.16, 127.28, 126.77, 126.52, 125.60, 124.56, 123.37, 123.07, 122.00, 121.97, 121.91, 120.94, 120.80, 120.62, 120.38, 119.65, 119.17, 118.97, 118.92, 117.19, 117.17, 116.46, 116.34, 77.38, 77.26, 77.06, 76.75, 66.08, 31.47. Elemental analysis (%) calcd for $C_{60}H_{49}N_3O_2$: C 85.98, H 5.61, N 4.77, O 3.64. Found: C 85.72, H 5.62, N 4.78.

3. Results and discussion

3.1 One-photon absorption

The one-photon absorption spectra of **SPF-1** and **SPF-2** in various organic solvents were investigated. The maximum absorption wavelength of **SPF-2** is longer than that of **SPF-1** (Table 1), which can be attributed to the incorporation of a diphenylaminoarylvinyl group into the spirobifluorene core of **SPF-2**. It can be seen from Table 1 that the absorption spectra of **SPF-1** and **SPF-2** exhibit almost no change with different polar solvents. However, the water content has a significant effect on the absorption response of the two compounds. It was noted that the absorption spectra of **SPF-1** in the DMF/water and **SPF-2** in 1,4-dioxane/water mixtures were all red-shifted and broadened.

Table 1 One-photon absorption properties of **SPF-1** and **SPF-2**

Compound	SPF-1				SPF-2			
Solvent	Toluene	THF	DCM	DMF	Toluene	THF	DCM	DMF
λ_{max} (nm)	362	360	363	361	397	396	398	400

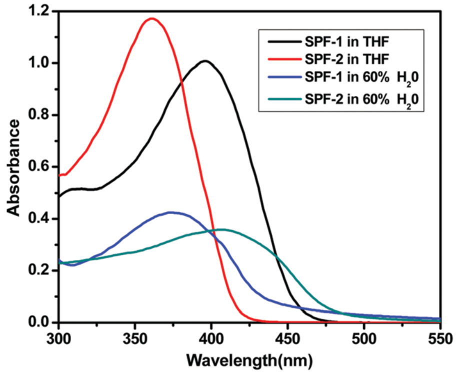

Fig. 1 One-photon absorption spectra of **SPF-1** and **SPF-2** in THF and organic solvent/water mixtures (60% water in volume).

In addition, the absorbance of **SPF-1** and **SPF-2** decreases with the increase of the water content (Fig. 1), respectively. The phenomena may be caused by the formation of their nanoaggregates.[23,24]

3.2 AIEE properties

SPF-1 and **SPF-2** are soluble in common organic solvents (such as toluene, THF, dichloromethane, 1,4-dioxane and DMF), but insoluble in pure water. We used anhydrous DMF as a good solvent and water as a poor solvent to investigate the AIEE attributes of **SPF-1** by the precipitation method.[23,25] **SPF-1** exhibited a relatively weak fluorescence emission (excited at 362 nm) in DMF solution (10 μM). As shown in Fig. 2, the fluorescence emission of **SPF-1** began to increase when the water was added slowly. When the water content reached 50%, a significant fluorescent enhancement (at 538 nm) could be observed. At a water content of more than 60%, the fluorescence emission intensity reached the maximum (Fig. 2, right). Increasing water fractions can reduce the solubility of **SPF-1** and the formation of **SPF-1** aggregates in the DMF/water mixture was confirmed using dynamic light scattering (DLS) analysis (Fig. S1, ESI†). In the aggregated state, the intramolecular rotations are restricted, which blocks the nonradiative relaxation channel and actives the radiative decay.[7] Apparently, the emission enhancement was caused by aggregation-induced effects. However, a further increase in the water content (>80%) caused the AIEE properties to undergo a slight decrease in the PL intensity. This phenomenon could be caused by the variation in the packing mode of the molecules in the aggregates.[23,26]

Similar AIEE properties were obtained for **SPF-2**. When excited at 400 nm, **SPF-2** emits weak fluorescence in pure 1,4-dioxane solution (10 μM). Addition of water into the 1,4-dioxane solution, however, aggregates the **SPF-2** molecules and enhances the fluorescence emission intensity (at 540 nm) (Fig. 3, left). **SPF-2** gave a maximum luminescence at f_w = 60% (Fig. 3, right). Compared to **SPF-1**, a more significant fluorescence enhancement was observed for **SPF-2** when the water content was increased from 40% to 50% in volume. This result can presumably be attributed to the comparatively lower solubility of **SPF-2** in the aqueous mixture. Thus, it can be confirmed that **SPF-1** and **SPF-2** were endowed with AIEE attributes.[27]

This journal is © The Royal Society of Chemistry 2019

Published on 21 January 2019. Downloaded on 2/12/2026 3:28:52 PM.

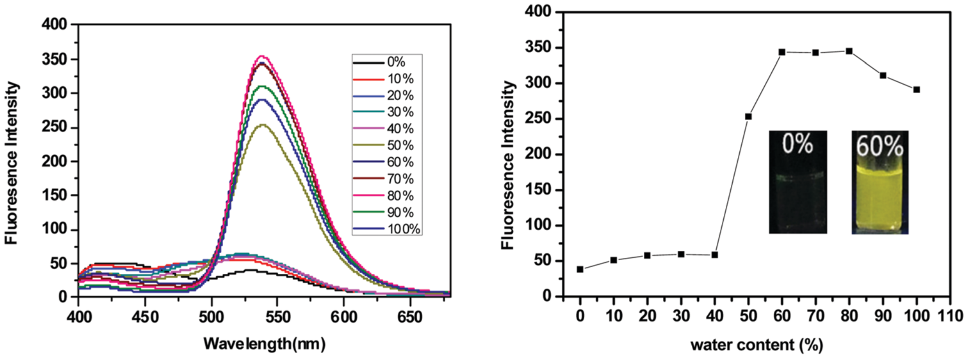

Fig. 2 Emission spectra of **SPF-1** in DMF and DMF/water mixtures with different water fractions (left). Plot of the emission intensity (*I*) *versus* the composition of the aqueous mixtures of the **SPF-1** DMF solution (right). Solution concentration: 10 μM; λ_{ex}: 362 nm. Inset (right): photographs of **SPF-1** in pure DMF and DMF/water mixtures (60%) under 365 nm UV irradiation.

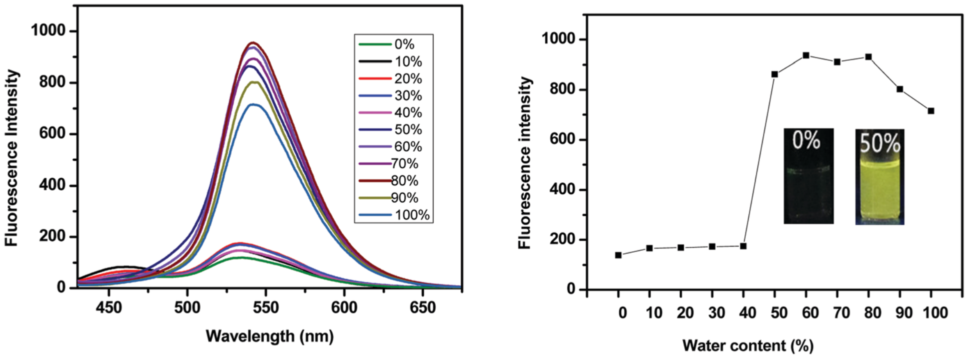

Fig. 3 Emission spectra of **SPF-2** in 1,4-dioxane and 1,4-dioxane/water mixtures with different water fractions (left). Plot of the emission intensity (*I*) *versus* the composition of the aqueous mixtures of **SPF-2** DMF solution (right). Solution concentration: 10 μM; λ_{ex}: 400 nm. Inset (right): photographs of **SPF-2** in pure 1,4-dioxane and 1,4-dioxane/water mixtures (50%) under 365 nm UV irradiation.

3.3 Excited-state intramolecular proton transfer characteristics of SPF

The process of excited-state intramolecular proton transfer (ESIPT) consists of proton transfer between an enol (E*) and a keto form (K*) upon photoexcitation (Scheme 2).[28–31] In general, an ESIPT-based luminophore shows dual emission bands: the normal emission from the enol-form (high energy, low Stokes shift) and the ESIPT emission from the keto-form (low energy, large Stokes shift).[30,32,33] AIE mechanisms involving ESIPT have been reported in the literature.[30,32] In the aggregate state, the keto emission used to be the preferred emission owing to strong intramolecular hydrogen bonding and other favorable parameters.[32,34,35] In the DMF/H_2O mixture (Fig. 2, left), **SPF-1** showed dual weak emissions at a lower fraction of water (0–40%), in which the shorter-wavelength emission occurred at 425 nm and the longer-wavelength emission occurred at 528 nm (excitation at 362 nm). As the ratio of water increased from 50% to 100%, the emission at 528 nm becomes the more prominent emission and is associated with the red-shift to 538 nm. The red shift of the emission band could be attributed to the result of aggregation-induced charge-transfer enhancement.[36–38] A similar trend was observed for compound **SPF-2** (Fig. 3, left). It showed weak fluorescence at 460 nm (enol emission) and 530 nm (keto emission) in a 1,4-dioxane/water mixture with water fractions ranging from 0 to 40 vol%. Upon increasing the amount of water to more than 40%, the fluorescence intensity of the shorter-wavelength emission (460 nm) disappeared completely, while that of the longer-wavelength emission (530 nm) increased significantly with a red shift from 530 to 542 nm.

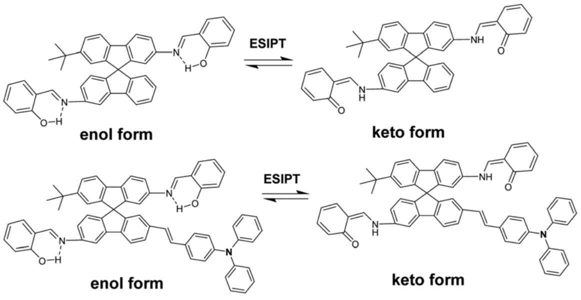

Scheme 2 Illustration of the ESIPT process for **SPF-1** and **SPF-2**.

To gain a better understanding of the ESIPT phenomena of **SPF-1** and **SPF-2**, a theoretical calculation based on density functional theory (DFT) and time-dependent density functional theory (TDDFT) methods was carried out using the Gaussian 16 program. The geometry optimizations of the S_0 and S_1 states were performed with the B3LYP hybrid DFT and the basis set

Published on 21 January 2019. Downloaded on 2/12/2026 3:28:52 PM.

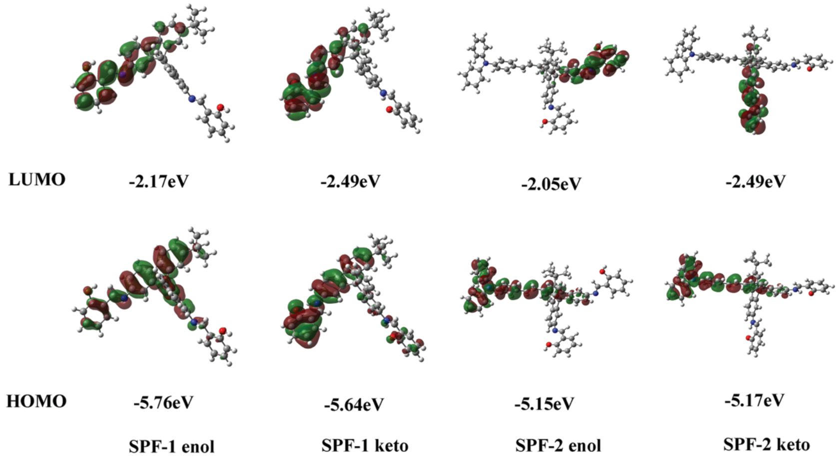

Fig. 4 The calculated frontier molecular orbitals for the HOMO and LUMO and the orbital energies of **SPF-1** and **SPF-2** in DMF.

used was 6-31G*. DMF was employed as solvent. Fig. 4 displays the highest occupied molecular orbital (HOMO) and the lowest unoccupied molecular orbital (LUMO) diagrams for the two compounds, and the calculated HOMO and LUMO energies are correspondingly listed. It is noteworthy that for **SPF-1** and **SPF-2**, the K* form is more stable than the E* form by more than 0.32 eV.[39] Therefore, the E* → K* transformation could occur through a barrier-less path owing to the lack of energy barrier in the S_1 excited state.[40] After decaying to the ground state, a reverse proton transfer process from the keto to the enol takes place to produce the original E form. For **SPF-2**, the occurrence of the reverse proton transfer process is not as easy because of the existence of the 0.4 kcal mol^{-1} (0.02 eV) energy barrier.[40] This result implied that the ESIPT process was feasible in the **SPF-1** and **SPF-2** molecules.

Moreover, the fluorescence properties of **SPF-1** and **SPF-2** in the enol and keto forms in DMF were simulated. The obtained fluorescence peaks of **SPF-1**-enol and **SPF-1**-keto are 404.4 and 522.72 nm, which is in excellent agreement with the experimental data of 425 and 528 nm (see Fig. 2, left). In the calculated fluorescence peaks of **SPF-2**, the emission bands 521.24 and 600.73 nm correspond to the enol and keto forms of **SPF-2**, respectively.[41] However, only a single emission band at 495 nm was observed in the experimental data. The average absolute deviation between the theoretical (521.24 nm) and experimental (495) wavelengths was found to be 26.24 nm. The longer-wavelength emission band of **SPF-2** (>495 nm) disappeared in DMF, which may be caused by the presence of intermolecular hydrogen bonding between the **SPF-2** and DMF molecules. The enol isomer of **SPF-2** is better stabilized by DMF molecules than the keto isomer and the ESIPT process is not possible.[40]

The time-resolved fluorescence decay behaviors of **SPF-1** (in DMSO/water solution, 9 : 1, v/v) and **SPF-2** (in 1,4-dioxane/water solution, 13 : 7, v/v) were investigated (Fig. S2 and S3, ESI†). Two relaxation pathways are involved in the decay process. The quick decay lifetimes are 3.63 and 0.82 ns, respectively, while the long decay lifetimes are 37.30 and 2.75 ns, respectively.[30] Therefore the ESIPT emission of **SPF-1** and **SPF-2** was further confirmed.

3.4 Detection of Zn^{2+}

The corresponding solutions of **SPF-1** in DMF/H_2O (9 : 1, v/v, 10 μM) and **SPF-2** in 1,4-dioxane/water (13 : 7, v/v, 10 μM) were prepared, respectively, in which the water volume percentage was less than 40% and the probe did not exhibit AIEE activity on its own.[9]

As depicted in Fig. 5, the **SPF** solutions show very weak fluorescence in the absence of Zn^{2+}.[42] Upon addition of Zn^{2+},

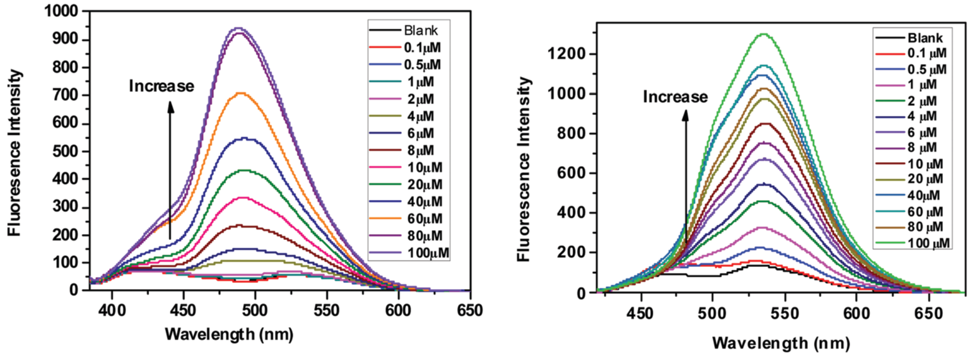

Fig. 5 Fluorescence spectra of **SPF-1** (10 μM) (λ_{ex} = 362 nm) with varying concentrations of Zn^{2+} in DMF/H_2O (9 : 1, v/v) (left). Fluorescence spectra of **SPF-2** (10 μM) (λ_{ex} = 400 nm) with varying concentrations of Zn^{2+} in 1,4-dioxane/H_2O (13 : 7, v/v) (right).

This journal is © The Royal Society of Chemistry 2019

Published on 21 January 2019. Downloaded on 2/12/2026 3:28:52 PM.

the fluorescence started to increase gradually. Fig. 5 shows the variation of the fluorescence intensity (at 488 nm for **SPF-1**, and at 536 nm for **SPF-2**) *versus* the amount of Zn^{2+} added to the solution. The increase in the fluorescence intensity was directly proportional to the Zn^{2+} concentration from 0.5 to 20 μM with a linear coefficient of 0.996 for **SPF-1** (Fig. S4, left, ESI†) and from 0 M to 4 μM with a linear coefficient of 0.991 for **SPF-2** (Fig. S4, right, ESI†), respectively. Thus, compounds **SPF-1** and **SPF-2** can be regarded as new off–on fluorescence sensors for Zn^{2+}. The detection limits (LOD) were found to be 300 nM for **SPF-1** and 63 nM for **SPF-2**, respectively. The LOD of **SPF-2** for Zn^{2+} was significantly lower than most of the previously reported systems.[5,9,43–49]

The absorption spectra of **SPF-1** and **SPF-2** were also recorded after the addition of Zn^{2+}. As depicted in Fig. 6 (left), the absorptions around 362 nm of **SPF-1** decreased and red-shifted gradually with an increase of the Zn^{2+} concentration, generating an isobestic point (at around 394 nm) simultaneously. Similar changes in the UV-vis spectra of **SPF-2** were observed and an isosbestic point appeared at around 436 nm (Fig. 6, right). These spectral changes could be attributed to the coordination of **SPF** toward Zn^{2+}.[43]

The selectivity of **SPF** toward Zn^{2+} was checked against other common cations (Ag^+, Al^{3+}, Ba^{2+}, Cd^{2+}, Co^{2+}, Fe^{3+}, Cu^{2+}, Hg^{2+}, Li^+, Mg^{2+}, Mn^{2+}, Ni^{2+} and Pb^{2+}). The free **SPF** showed a weak fluorescence emission (Fig. 7). Upon the addition of various metal ions to the solution of **SPF**, the fluorescence emission of **SPF** exhibited negligible changes. However, Zn^{2+} caused a significant fluorescent enhancement either in the presence (Fig. 8 and 9) or absence (Fig. 7) of competitive ions such as Ag^+, Al^{3+}, Ba^{2+}, Cd^{2+}, Co^{2+}, Fe^{3+}, Li^+, Mg^{2+}, Mn^{2+}, Ni^{2+} and Pb^{2+}. An obvious color change induced by Zn^{2+} can be observed under 365 nm UV irradiation (Fig. S5 and S6, ESI†). As depicted in Fig. 8, Cu^{2+} and Hg^{2+} exert interference on the fluorescence detection of Zn^{2+} with probe **SPF-1**. The coexistence of the Cu^{2+} and Hg^{2+} ions did not have an obvious impact on the fluorescence intensity of **SPF-2** (Fig. 9), revealing that **SPF-2** is highly selective for Zn^{2+}. It is worth mentioning that **SPF-1** displayed different absorbance responses for Cu^{2+}, Hg^{2+} and Zn^{2+} (Fig. 10). After the addition of Cu^{2+}, **SPF-1** showed an obvious color change from colorless to light yellow (Fig. 10, inset). These phenomena can guarantee the high selectivity of the probe **SPF-1** for Zn^{2+} in solution. Additionally, Hg^{2+} and Cu^{2+} are present in relatively low concentrations *in vivo*,[42,50] and the interferences from them for the detection of Zn^{2+} in cells or tissues can be neglected.

3.5 Proposed sensing mechanism of SPF toward Zn^{2+}

Up until now, several mechanisms for sensing Zn^{2+} such as metal–ligand charge transfer (MLCT), chelation enhanced

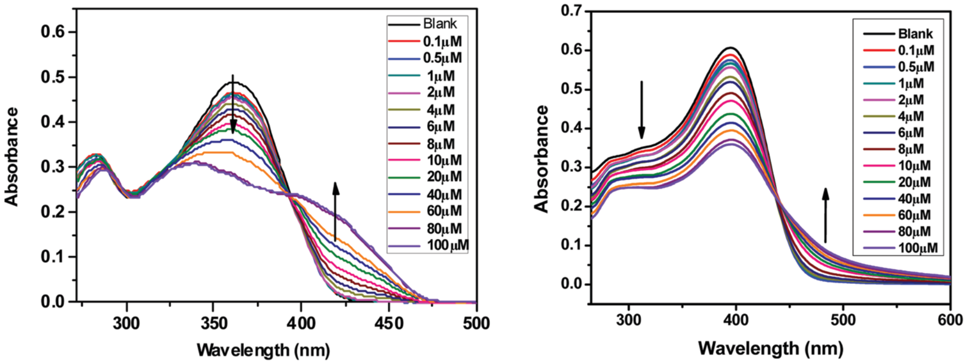

Fig. 6 Absorption spectra for **SPF-1** (10 μM) with varying concentrations of Zn^{2+} in DMF/H_2O (9 : 1, v/v) (left). Absorption spectra for **SPF-2** (10 μM) with varying concentrations of Zn^{2+} in 1,4-dioxane/H_2O (13 : 7, v/v) (right).

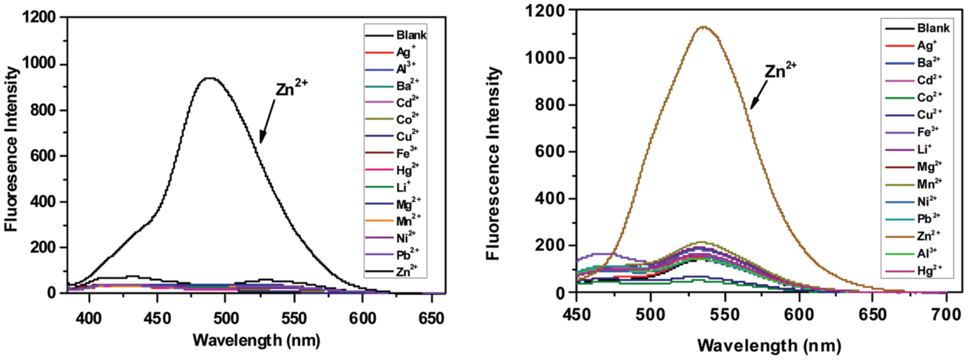

Fig. 7 The fluorescence spectra for **SPF-1** (10 μM) upon addition of various metal ions (10 μM) in DMF/H_2O (9 : 1, v/v) (left). The fluorescence spectra for **SPF-2** (10 μM) upon addition of various metal ions (10 μM) in 1,4-dioxane/H_2O (13 : 7, v/v) (right).

This journal is © The Royal Society of Chemistry 2019

Published on 21 January 2019. Downloaded on 2/12/2026 3:28:52 PM.

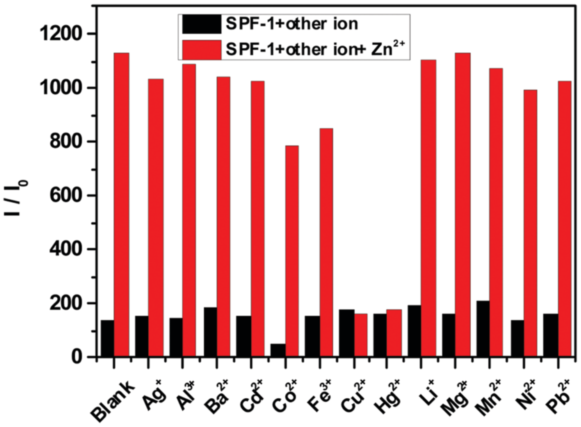

Fig. 8 The relative fluorescence intensity profiles (I/I_0) of **SPF-1** (10 μM, DMF/H_2O, 9 : 1, v/v) in the presence of 1 equiv. Zn^{2+} and the interfering ions (Ag^+, Al^{3+}, Ba^{2+}, Cd^{2+}, Co^{2+}, Fe^{3+}, Cu^{2+}, Hg^{2+}, Li^+, Mg^{2+}, Mn^{2+}, Ni^{2+}, Pb^{2+}, respectively). Red bars: the addition of Zn^{2+} and various other metal ions. Black bars: the addition of various other metal ions.

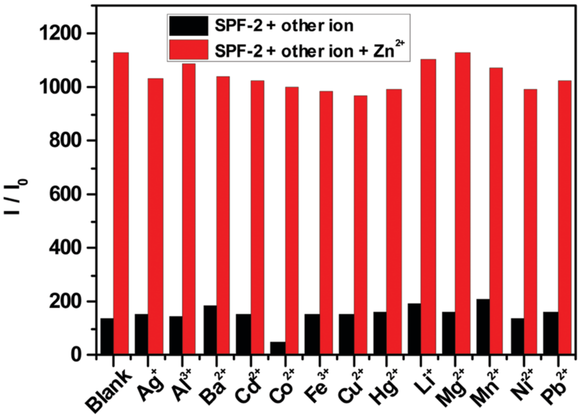

Fig. 9 The relative fluorescence intensity profiles (I/I_0) of **SPF-2** (10 μM, 1,4-dioxane/H_2O, 13 : 7, v/v) in the presence of 1 equiv. Zn^{2+} and the interfering ions (Ag^+, Al^{3+}, Ba^{2+}, Cd^{2+}, Co^{2+}, Fe^{3+}, Cu^{2+}, Hg^{2+}, Li^+, Mg^{2+}, Mn^{2+}, Ni^{2+}, Pb^{2+}, respectively). Red bars: the addition of Zn^{2+} and various other metal ions. Black bars: the addition of various other metal ions.

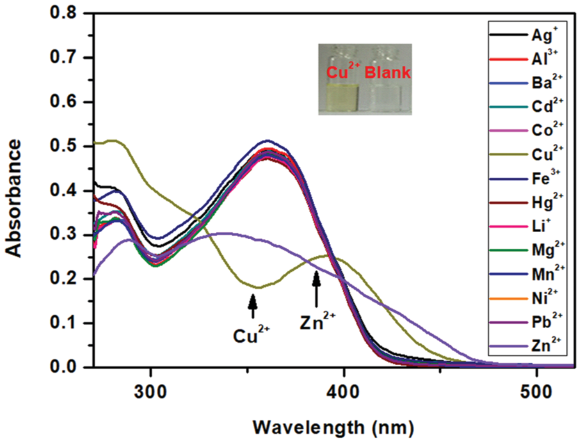

Fig. 10 The absorption spectra of **SPF-1** (10 μM) upon addition of various metal ions (10 μM) in DMF/H_2O (9 : 1, v/v).

fluorescence (CHEF), photoinduced electron transfer (PET), and C=N isomerization have been reported.[9]

The coordination of **SPF** with Zn^{2+} was confirmed by HRMS analysis. The reaction mixture of probe **SPF-2** with Zn^{2+} exhibited a prominent peak at *m*/*z* 950.7093 (Fig. S8, ESI†), which is assigned to the species [**SPF-2** + $2Zn^{2+}$ − $C(CH_3)_3$]. As shown in Fig. S7 (ESI†), the molecular ion peaks corresponding to [**SPF-1** + $2Zn^{2+}$ − $C(CH_3)_3$ − 2H] at *m*/*z* 679.4360, [**SPF-1** + $2Zn^{2+}$ − $2CH_3$ + H] at *m*/*z* 709.4486, and [**SPF-1** + $2Zn^{2+}$ − CH_3] at *m*/*z* 723.4612 could be clearly observed. To expound the reason for the fluorescence light-up, DLS analysis was performed. As depicted in Fig. 11, the intensity-average hydrodynamic diameter, $\langle D_h \rangle$, of **SPF** is approximately 2.0 nm, which is in line with the molecular size. This indicates that **SPF-1** can be molecularly dissolved in DMF/water and **SPF-2** can be dissolved in a 1,4-dioxane/water mixture, respectively. However, the mean diameter was approximately 12 nm for **SPF-1** and 193 nm for **SPF-2** upon introduction of 2 equivalents of Zn^{2+}. Increasing the concentration of Zn^{2+} resulted in a significant enhancement in the average size of the aggregates (Fig. 11) and the fluorescence intensity, which supports the observed Zn^{2+}-triggered AIEE activity of the **SPF** probe.[9,51] The formation of aggregates can also be confirmed by the observation of a long absorption tail (see Fig. 6). On the basis of the experimental results described above, we proposed that the phenomenon caused by the addition of Zn^{2+} and resulting in the fluorescence enhancement could be attributed to the following reasons: (1) the coordination of **SPF** with Zn^{2+} can reduce the solubility of **SPF** and induce the formation of **SPF** aggregates; (2) the ESIPT process can be suppressed through a metal ion binding process;[52–56] (3) the binding of the nitrogen atom of C=N with Zn^{2+} restricted C=N isomerization in the excited states and inhibited the PET process of the C=N group within **SPF**.[43]

3.6 pH effect

We investigated the effect of pH on the sensing behavior of **SPF** towards Zn^{2+}. The variation of the fluorescence intensity with different pH values in the absence and presence of Zn^{2+} are shown in Fig. 12.

The fluorescence intensity of pure **SPF-1** (at 488 nm) remains almost unchanged in a wide pH range of 3–13. After addition of 1 equivalent of Zn^{2+}, the fluorescence intensity of **SPF-1** is enhanced gradually when the pH is increased from 3.0 to 6.1. At pH 6.1, the fluorescence intensity reached a plateau and did not change significantly upon changing the pH values from 6.1 to 10.5. At pH values higher than 10.5, a slight decline in the emission occurred, which could be attributed to the formation of $Zn(OH)_2$.[42] In strong acidic solutions ($pH < 3.0$), the introduction of Zn^{2+} caused no changes in the fluorescence intensity of **SPF-1**, which could be attributed to the instability of the C=N bond under low pH value conditions.[3]

In acidic environments ($pH < 6.0$), the fluorescence of pure **SPF-2** (at 535 nm) increased significantly, which could be due to the suppressed PET processes from the protonated triphenylamine unit.[6] When the pH increased from 6.1 to 7.4, a slight decline in the emission can be observed. In basic conditions ($pH > 7.4$),

Published on 21 January 2019. Downloaded on 2/12/2026 3:28:52 PM.

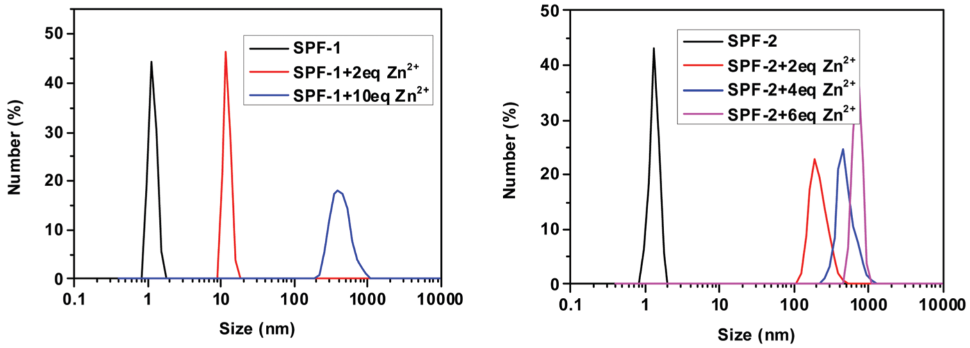

Fig. 11 DLS profile for **SPF-1** (left) (50 μM in aqueous solution) and in the presence of 2.0 equiv. of Zn^{2+}, and 10.0 equiv. of Zn^{2+}, respectively. DLS profile for **SPF-2** (right) (50 μM in aqueous solution) and in the presence of 2.0 equiv. of Zn^{2+}, 4.0 equiv. of Zn^{2+}, and 6.0 equiv. of Zn^{2+}, respectively.

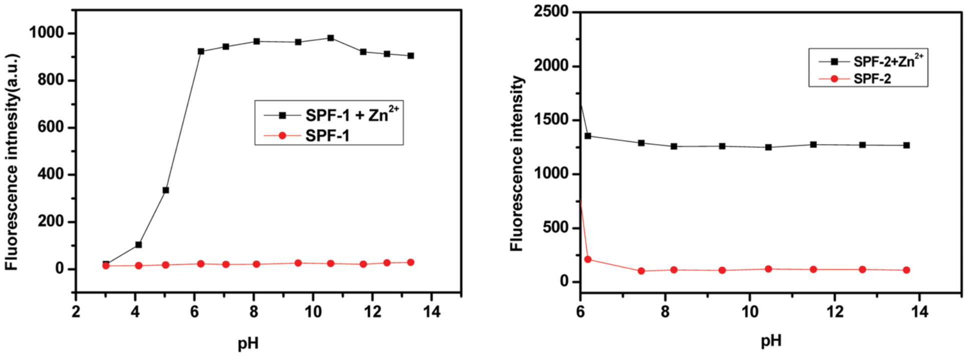

Fig. 12 Variation of fluorescence intensity at 488 nm for **SPF-1** solution with and without Zn^{2+} (1 equiv.) as a function of pH (left). Variation of fluorescence intensity at 535 nm for **SPF-2** solution with and without Zn^{2+} (1 equiv.) as a function of pH (right).

almost no changes in the fluorescence intensity were found. In a pH greater than 6.1, the emission intensity of **SPF-2** increased dramatically after addition of 1 equivalent of Zn^{2+}. The pH study shows that SPF could be used to monitor Zn^{2+} at a wide range of pH values and has the potential for application in conditions with a physiological pH (6.0–9.0).[9]

3.7 Two-photon absorption properties of SPF-2

In the structure of **SPF-2**, the triphenylamine group functions as an electron donor (D), the 2-(iminomethyl)phenol moiety acts as an electron acceptor (A) and the fluorene-vinyl moiety as a conjugation bridge. Therefore, the biphenyl branch containing a triphenylamine group is a donor–π–acceptor (D–π–A) type chromophore and is expected to serve as a source for the two-photon absorption. The TPA cross-section value of **SPF-2** was determined using a femtosecond open-aperture Z-scan technique in THF.[23] The open Z-scan data are shown in Fig. 13 and the σ of **SPF-2** was found to be 200 GM at a wavelength of 800 nm.

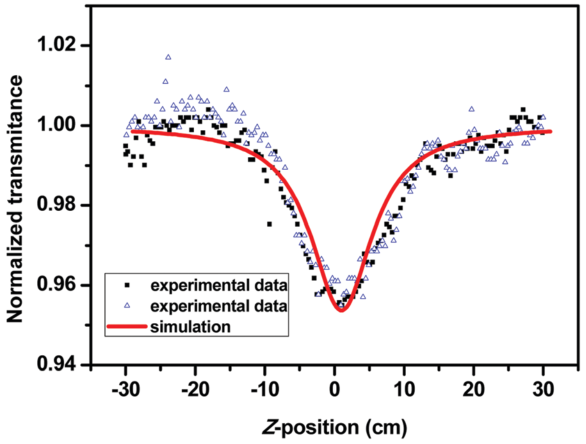

Fig. 13 Open *Z*-scan data of **SPF-2** in THF.

3.8 Cell imaging studies

The application of **SPF-1** for intracellular Zn^{2+} imaging (one-photon fluorescence) and **SPF-2** for two-photon fluorescence cell imaging were demonstrated, respectively. Before this, the cytotoxicities of **SPF-1** and **SPF-2** were first evaluated using MTT assays. After incubating the A549 cells with 50 μM **SPF-1** or **SPF-2** for 24 h, the cell viability remained at more than 95%, indicating the low cytotoxicity of the probe.[57]

Almost no intracellular fluorescence was observed for the **SPF-1** endocytosed cells. However, an intense green fluorescence was detected after these cells were treated with 100 μM Zn^{2+} solutions (Fig. 14). The results of this experiment indicated that **SPF-1** is potentially applicable for use in intracellular Zn^{2+} imaging.[3]

Two-photon excited fluorescence microscopy is a powerful method that is used for three-dimensional imaging in biological

Published on 21 January 2019. Downloaded on 2/12/2026 3:28:52 PM.

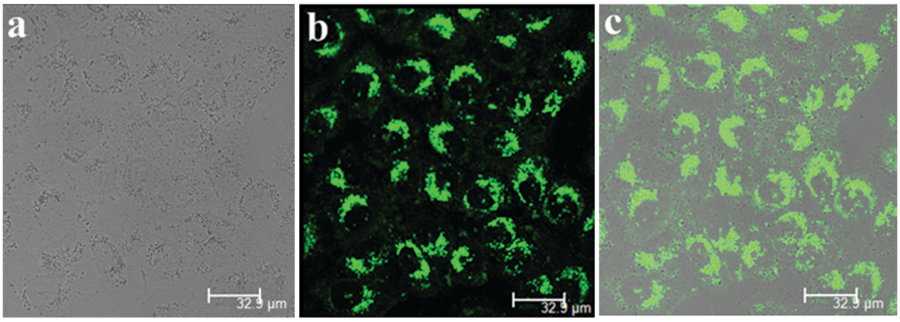

Fig. 14 Confocal fluorescence images of A549 cells after incubation with **SPF-1** (50 μM) for 30 min, and upon further incubation with Zn^{2+} (100 μM) for another 30 min. (a) Bright-field transmission image; (b) fluorescence image; and (c) overlay images of the A549 cells.

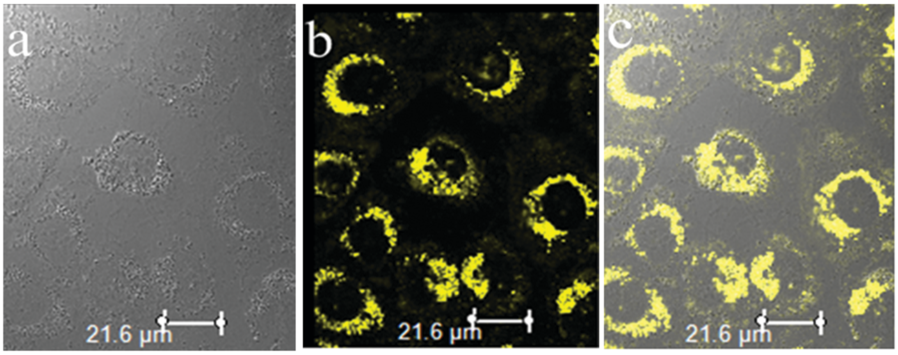

Fig. 15 Two-photon fluorescence images (at 800 nm) for A549 cells incubated with **SPF-2** (50 μM) for 30 min. (a) Bright field; (b) fluorescence; and (c) overlay images of the A549 cells.

systems owing to several distinct advantages, such as an increased penetration depth, lower tissue auto-fluorescence and self-absorption, and so on. The A549 cells treated with **SPF-2** (50 μM) show a bright yellow fluorescence using two-photon microscopy (at 800 nm) (Fig. 15). The results proved that **SPF-2** is suitable for two-photon fluorescence imaging of cells. As **SPF-2** is more hydrophobic than **SPF-1**, the **SPF-2** molecules aggregate more easily in the intracellular environment and emit a strong fluorescence signal.

4. Conclusions

In summary, two spirobifluorene-based probes for Zn^{2+} have been developed by taking advantage of their AIEE features. The sensing mechanism is ascribed to the chelation mediated AIEE behavior of **SPF**. **SPF-1** was successfully used for intracellular Zn^{2+} imaging and **SPF-2** was used for two-photon fluorescence cell imaging. The results demonstrated that spirobifluorene is an ideal building block for AIEE-based bioprobes. We hope that this molecular design triggers further interest in using spiro-configured compounds in AIEE-based bioprobes for further applications.

Conflicts of interest

There are no conflicts to declare.

Acknowledgements

This work was financially supported by the Ministry of Education of China (PCSIRT_IRT_16R49) and the Shanghai Government (18DZ2254200).

Notes and references

1 S. H. Jung, K.-Y. Kwon and J. H. Jung, *Chem. Commun.*, 2015, **51**, 952.
2 R. K. Pathak, V. K. Hinge, A. Rai, D. Panda and C. P. Rao, *Inorg. Chem.*, 2012, **51**, 4994.
3 H. Liu, Y. Dong, B. Zhang, F. Liu, C. Tan, Y. Tan and Y. Jiang, *Sens. Actuators, B*, 2016, **234**, 616.
4 M. P. Cuajungco and G. J. Lees, *Neurobiol. Dis.*, 1997, **4**, 137.
5 K. Tayade, S. K. Sahoo, B. Bondhopadhyay, V. K. Bhardwaj, N. Singh, A. Basu, R. Bendre and A. Kuwar, *Biosens. Bioelectron.*, 2014, **61**, 429.
6 H.-J. Lee, C.-W. Cho, H. Seo, S. Singha, Y. W. Jun, K.-H. Lee, Y. Jung, K.-T. Kim, S. Park, S. C. Baed and K. H. Ahn, *Chem. Commun.*, 2016, **52**, 124.
7 R. Hu, J. L. Maldonado, M. Rodriguez, C. Deng, C. K. W. Jim, J. W. Y. Lam, M. M. F. Yuen, G. Ramos-Ortiz and B. Z. Tang, *J. Mater. Chem.*, 2012, **22**, 232.
8 R. Liu, M. Shu, J. Hu, S. Zhu, H. Shi and H. Zhu, *Dyes Pigm.*, 2017, **137**, 174.

Published on 21 January 2019. Downloaded on 2/12/2026 3:28:52 PM.

9 M. Shyamal, P. Mazumdar, S. Maity, S. Samanta, G. P. Sahoo and A. Misra, *ACS Sens.*, 2016, **1**, 739.

10 Y. Wang, G. Lai, Z. Li, Y. Ma, Y. Shen and C. Wang, *Tetrahedron*, 2015, **71**, 2761.

11 S. Kim, T. Y. Ohulchanskyy, H. E. Pudavar, R. K. Pandey and P. N. Prasad, *J. Am. Chem. Soc.*, 2007, **129**, 2669.

12 W. Huang, F. Tang, B. Li, J. Su and H. Tian, *J. Mater. Chem. C*, 2014, **2**, 1141.

13 Q. Ye, S. Chen, D. Zhu, X. Lu and Q. Lu, *J. Mater. Chem. B*, 2015, **3**, 3091.

14 X. Zhang, X. Gan, S. Yao, W. Zhu, J. Yu, Z. Wu, H. Zhou, Y. Tian and J. Wu, *RSC Adv.*, 2016, **6**, 60022.

15 J. Li, T. Liu, M. Zheng, M. Sun, D. Zhang, H. Zhang, P. Sun, S. Xue and W. Yang, *J. Phys. Chem. C*, 2013, **117**, 8404.

16 Y.-J. Dong, Z. Meng, C.-L. Ho and W.-Y. Wong, *Tetrahedron*, 2017, **73**, 3305.

17 L.-Y. Lin, X.-Y. Lin, F. Lin and K.-T. Wong, *Org. Lett.*, 2011, **13**, 2216.

18 H. Xiao, Y. Zhang, W. Zhang, S. Li and R. Xu, *Sens. Actuators, B*, 2016, **233**, 469.

19 H. Xiao, Y. Zhang, S. Li, W. Zhang, Z. Han, J. Tan, S. Zhang and J. Du, *Sens. Actuators, B*, 2016, **236**, 233.

20 Z. Han, J. Tan, T. Wei, Y. Zhang, H. Xiao, L. Xu and B. He, *Sens. Actuators, B*, 2018, **255**, 2290.

21 H. Xiao, H. Yin, L. Wang, C. Mei and X. Zhang, *Monatsh. Chem.*, 2012, **143**, 683.

22 Y.-C. Wang, H. Zhou, J.-L. Ding, Q. Chen, H.-B. Xiao, X.-M. Tao and S.-X. Qian, *Chin. Phys. Lett.*, 2010, **27**(3), 038201.

23 T. Jiang, Y. Qu, B. Li, Y. Gao and J. Hua, *RSC Adv.*, 2015, **5**, 1500.

24 R. S. Yoshii, A. S. Nagai, K. Z. Tanaka and Y. S. K. Chujo, *Chem. – Eur. J.*, 2013, **19**, 4506.

25 K. Supattarasakda, K. Petcharoen, T. Permpool, A. Sirivat and W. Lerdwijitjarud, *Powder Technol.*, 2013, **249**, 353.

26 G. J. Tian, W. Huang, S. Y. Cai, H. T. Zhou, B. Li, Q. C. Wang and J. H. Su, *RSC Adv.*, 2014, **4**, 38939.

27 X. Wang, J. Hu, T. Liu, G. Zhang and S. Liu, *J. Mater. Chem.*, 2012, **22**, 8622.

28 P. Kaewmati, Y. Yakiyama, H. Ohtsu, M. Kawano, S. Haesuwannakij, S. Higashibayashid and H. Sakurai, *Mater. Chem. Front.*, 2018, **2**, 514.

29 J. Massue, D. Jacquemin and G. Ulrich, *Chem. Lett.*, 2018, **47**, 1083.

30 L. Yan, T. Qing, R. Li, Z. Wang and Z. Qi, *RSC Adv.*, 2016, **6**, 63874.

31 Z. A. Kowser, U. Rayhan, S. Rahman, P. E. Georghiou and T. Yamato, *Tetrahedron*, 2017, **73**, 5418.

32 Q. Chen, C. Jia, Y. Zhang, W. Du, Y. Wang, Y. Huang, Q. Yang and Q. Zhang, *J. Mater. Chem. B*, 2017, **5**, 7736.

33 J. Jayabharathi, P. Ramanathan, V. Thanikachalam and A. Arunpandiyan, *J. Fluoresc.*, 2014, **24**, 827.

34 P. Singh, H. Singh, R. Sharma, G. Bhargava and S. Kumar, *J. Mater. Chem. C*, 2016, **4**, 11180.

35 V. S. Padalkar and S. Seki, *Chem. Soc. Rev.*, 2016, **45**, 169.

36 R. Yoshii, A. Hirose, K. Tanaka and Y. Chujo, *Chem. – Eur. J.*, 2014, **20**, 8320.

37 X. Wang, Y. Wu, Q. Liu, Z. Li, H. Yan, C. Ji, J. Duan and Z. Liu, *Chem. Commun.*, 2015, **51**, 784.

38 Q. Liu, X. Wang, H. Yan, Y. Wu, Z. Li, S. Gong, P. Liu and Z. Liu, *J. Mater. Chem. C*, 2015, **3**, 2953.

39 J. Massuea, A. Felouata, M. Curtila, P. M. Vérité, D. Jacqueminb and G. Ulricha, *Dyes Pigm.*, 2019, **160**, 915.

40 N. Klinhoma, N. Saengsuwan, S. Sriyab, P. Prompinit, S. Hannongbua and S. Suramitr, *Spectrochim. Acta, Part A*, 2019, **206**, 359.

41 C. Sun, H. Li, H. Yin, Y. Li and Y. Shi, *J. Mol. Liq.*, 2018, **269**, 650.

42 F. Sun, G. Zhang, D. Zhang, L. Xue and H. Jiang, *Org. Lett.*, 2011, **13**, 6378.

43 J.-C. Qin, L. Fan and Z.-Y. Yang, *Sens. Actuators, B*, 2016, **228**, 156.

44 M. Hosseini, A. Ghafarloo, M. R. Ganjali, F. Faridbod, P. Norouzi and M. S. Niasari, *Sens. Actuators, B*, 2014, **198**, 411.

45 A. K. Mahapatra, S. K. Manna, C. D. Mukhopadhyay and D. Mandal, *Sens. Actuators, B*, 2014, **200**, 123.

46 J.-H. Hu, J.-B. Li, J. Qi and Y. Sun, *Sens. Actuators, B*, 2015, **208**, 581.

47 Y. R. Li, J. Wu, X. Jin, J. W. Wang, S. Han, W. Y. Wu, J. Xu, W. S. Liu, X. J. Yao and Y. Tang, *Dalton Trans.*, 2014, **43**, 1881.

48 K. Wechakorn, K. Suksen, P. Piyachaturawat and P. Kongsaeree, *Sens. Actuators, B*, 2016, **228**, 270.

49 E. J. Song, J. Kang, G. R. You, G. J. Park, Y. Kim, S.-J. Kim, C. Kim and R. G. Harrison, *Dalton Trans.*, 2013, **42**, 15514.

50 A. P. De Silva, H. Q. N. Gunaratne, T. Gunnlaugsson, A. J. M. Huxley, C. P. McCoy, J. T. Rademacher and T. E. Rice, *Chem. Rev.*, 1997, **97**, 1515.

51 Y. Gao, Y. Qu, T. Jing, H. Zhang, N. He, B. Li, J. Wu and J. Hua, *J. Mater. Chem. C*, 2014, **2**, 6353.

52 F. Huo, Q. Wu, J. Kang, Y. Zhang and C. Yin, *Sens. Actuators, B*, 2018, **262**, 263.

53 L. Tang, M. Cai, P. Zhou, J. Zhao, K. Zhong, S. Hou and Y. Bian, *RSC Adv.*, 2013, **3**, 16802.

54 M. M. Henary, Y. Wu and C. J. Fahrni, *Chem. – Eur. J.*, 2004, **10**, 3015.

55 L. Ma, G. Liu, S. Pu, C. Zheng and C. Fan, *Tetrahedron*, 2017, **73**, 1691.

56 T. Wei, G. Liang, X. Chen, J. Qi, Q. Lin, Y. Zhang and H. Yao, *Tetrahedron*, 2017, **73**, 2938.

57 Q. Hu, M. Gao, G. Feng, X. Chen and B. Liu, *ACS Appl. Mater. Interfaces*, 2015, **7**, 4875.